Bond-order potential for transition metal carbide cluster for the growth simulation of a single-walled carbon nanotube

Yasushi Shibuta[1]*, Shigeo Maruyama[2]

[1]*Department of Materials Engineering, The University of Tokyo*

7-3-1 Hongo, Bunkyo-ku, Tokyo 113-8656, Japan

[2]*Department of Mechanical Engineering, The University of Tokyo*

7-3-1 Hongo, Bunkyo-ku, Tokyo 113-8656, Japan

Abstract

A classical multi-body potential for transition metal carbide cluster is developed in the form of the bond-order type potential function. The parameter sets between carbon atoms and several transition metal atoms (Fe, Co and Ni) are constructed by fitting binding energies from Density Functional Theory (DFT) calculations. Using the potential function, clustering process of carbon atoms to a small metal cluster is studied by classical molecular dynamics (MD) simulation. The number of hexagonal rings in the Co cluster increases about twice as fast as in the Fe cluster. This implies that the graphitic lattice interacts more strongly with Co atoms than with Fe atoms. A Co cluster has a crystal structure where metal atoms are regularly allocated and embedded in the hexagonal carbon network in the simulation. In contrast, carbon atoms cover the entire surface in case of the Fe cluster. Additionally, the potential energy surface that a carbon atom feels from FCC metals is examined. The potential energy minima are distributed on the hexagonal network showing the FCC structure can be a template where a graphene is formed.

KeyWord: Molecular Dynamics Simualtion; Bond-order potential; Carbon nanotube; transition metal carbide cluster

*Corresponding Author. Fax: +81-3-5841-8653

E-mail address: shibuta@material.t.u-tokyo.ac.jp (Y. Shibuta)

1. Introduction

The formation mechanism of single-walled carbon nanotubes (SWNTs) [1] has been widely discussed since their discovery [2]. It is well known that catalytic metal atoms are essential to form SWNTs. Hence, understanding of the role of the catalytic metal atoms in the formation process is critical for future control of the diameter and chirality of SWNTs.

In earlier stages, there were many models that considered the role of the catalyst to be active at the atomic level such as the 'scooter model' [3]. Recently, there has been a growing number of experimental [4-7] and numerical [7-12] works on models based on the carbon-saturated metal cluster or liquid as a seed for SWNTs. In these models, carbon atoms precipitate, nucleate the cap structure and form the SWNT from the carbon-saturated metal cluster or liquid. This process is often referred to as the vapor-liquid-solid (VLS) model [13], and the carbon-metal alloy phase diagram [14] is often used to explain the VLS model. From an experimental point of view, transmission electron microscopy (TEM) images support the above idea [4-7]. However, the discussion only from the static structure is not enough. Hence, a theoretical approach based on dynamics is essential for the discussion of the formation process of SWNTs.

As a numerical approach, the molecular dynamics (MD) method gives us much information that cannot be seen in experimental approaches since it traces the motion of molecules directly. However, it is difficult to reproduce the entire formation process of SWNTs due to the computational limit. We have shown the numerical modeling of nucleation process of SWNTs from isolated carbon atoms and isolated metal atoms for the laser-furnace process [9] or from isolated carbon atoms and a transition metal cluster for the CCVD process [10] by classical MD simulations. In the latter simulation, the crystal structure of the transition metal atoms act as a template of hexagonal carbon network. On the other hand, Ding *et al.* [11] have shown a nucleation process focusing on the temperature gradient in the metal particle as a driving force of nucleation. Recently, Galli *et al.* [12] have discussed the initial nucleation process by an *ab initio* MD simulation.

Another debatable issue is the catalytic ability of transition metals. It is well known that the yield of SWNTs strongly depends on the transition metal used [2], however, the critical reason is still

unknown. The potential functions for transition metal atoms have been developed; Morse [15,16], Johnson [17], Finnis-Sinclair [18], EAM [19] and so on. On the other hand, there is no reliable classical potential function between carbon and transition metals available to this date. In this letter, classical multi-body potential functions between carbon atoms and transition metal atoms, as well as among transition metal atoms, are constructed. Using these potential functions, interactions between carbon atoms and several transition metals in the nucleation process are studied

2. Formulation of multi-body potential functions for classical MD simulations

Our approach for understanding of formation process of SWNTs is to use the classical molecular dynamics method for large systems and long time scale simulation. As for metal atoms, we have constructed classical potential functions between carbon clusters and three metal atoms (La, Sc and Ni) to simulate the formation process of endohedral metallofullerenes [20]. Here, parameter sets for multi-body potential functions between carbon atoms and three transition metals (Fe, Co and Ni) are constructed.

These functions have the covalent term based on a Brenner-type potential [21]; the parameters for three transition metals (Fe, Co and Ni) are constructed by fitting binding energies from Density Functional Theory (DFT) calculations to the following functions. Gaussian98 [22] is used for the following DFT calculation. Becke's three-parameter exchange functional with Lee-Yang-Parr correlation functional (B3LYP) [23,24] is applied. The effective core potentials (LANL2DZ) [25] is used for basis set.

Firstly, total energies of small symmetrical clusters MC_n and M_n (M = Fe, Co, Ni; n = 1-4) with various bond lengths are calculated (Fig. 1); the bond length is changed with keeping symmetrical structure at 0.05 Å intervals from 1.8 to 3.5 Å for metal-carbon clusters and from 1.5 to 3.0 Å for metal clusters, respectively. Optimized structures of the small cluster of transition metals have Jahn-Teller distortions which are asymmetry [26]. However, angular effect is neglected in our model for simplicity because binding energy depends much on the coordination number compared with the bonding angle. Various spin states are calculated for each cluster (2S+1; 1,3,5 for Ni_2, 13,5,7 for Co_2,

1,3,5,7,9 for Ni_3, Ni_4, Fe_2, 2,4,6,8 for Co_3 and 1,3,5,7,9,11,13 for Co_4, Fe_3) and its envelopes are adopted.

Next, total energies of an isolated carbon atom and of an isolated metal atom are calculated. For reducing the basis set superposition error (BSSE), dummy atoms are used for calculation of the energy of the isolated atom, i.e. all atoms except one are replaced with dummy atoms in the above small symmetrical clusters. As in the former process, bond lengths are changed symmetrically at 0.05 Å intervals from 1.8 to 3.5 Å for metal-carbon clusters with dummy atoms, and from 1.5 to 3.0 Å for metal clusters with dummy atoms.

The binding energy is then obtained from the difference of the above two energies. The obtained potential energies are fitted to the following functions.

$$E = V_{\mathrm{R}} - V_{\mathrm{A}} \tag{1}$$

$$V_{\mathrm{R}} = \frac{D_{\mathrm{e}}}{S-1}\exp\left\{-\beta\sqrt{2S}\,(r - R_{\mathrm{e}})\right\} \tag{2}$$

$$V_{\mathrm{A}} = B^{*}\frac{D_{\mathrm{e}}S}{S-1}\exp\left\{-\beta\sqrt{2/S}\,(r - R_{\mathrm{e}})\right\} \tag{3}$$

$$B^{*} = \left\{1 + b(N^{\mathrm{C}} - 1)\right\}^{\delta} \tag{4}$$

Here, r denotes the distance between a metal and a carbon atom or between two metal atoms. V_{R} and V_{A} are Morse-type repulsive and attractive terms, respectively. D_{e} and R_{e} are the binding energy and equilibrium bond length, respectively. Potential parameters S, β, b and δ determine the shape of the potential functions. For metal-carbon multi-body potential functions, the multi-body effect is included using an additional term B^{*}, which is expressed as a function of carbon coordination number of a metal atom N^{C}. For metal-metal interactions, the binding energy D_{e} and the equilibrium bond length R_{e} are expressed as direct functions of the metal coordination number N^{M} instead of using the additional term B^{*}.

$$D_{\mathrm{e}} = D_{\mathrm{e1}} + D_{\mathrm{e2}}\exp\left\{-C_D(N^{\mathrm{M}} - 1)\right\} \tag{5}$$

$$R_{\mathrm{e}} = R_{\mathrm{e1}} - R_{\mathrm{e2}}\exp\left\{-C_{\mathrm{R}}(N^{\mathrm{M}} - 1)\right\} \tag{6}$$

The coordination number N^{C} and N^{M} are defined using the cut-off function $f(r)$. Here, the effect of the

angle between bonds is ignored since it is much smaller than that of the coordination number.

$$f(r)=\begin{cases}1 & (r<R_1)\\ \left(1+\cos\dfrac{r-R_1}{R_2-R_1}\pi\right)/2 & (R_1<r<R_2)\\ 0 & (r>R_2)\end{cases} \tag{7}$$

$$N^{\mathrm{C}}{}_i = 1+\sum_{\text{carbon } k(\neq j)} f(r_{ik}) \tag{8}$$

$$N^{\mathrm{M}}{}_i = 1+\sum_{\text{metal } k(\neq j)} f(r_{ik}),\quad N^{\mathrm{M}}{}_{ij}=\frac{N^{\mathrm{M}}{}_i + N^{\mathrm{M}}{}_j}{2} \tag{9}$$

Figure 2(a) shows the binding energies between metal atoms from DFT calculation and fitted potential functions from the metal cluster M_n (M = Fe, Co, Ni; n = 2-4). The steepest descent method is used for fitting. In addition to these binding energies D_e and equilibrium bond lengths R_e, parameters of Morse Potential parameters[16] are used for the case of coordination number N^C = 12 (Co, Ni) and N^C = 8 (Fe) for fitting to equation (5) and (6), respectively. Figure 2(b) shows the binding energies between the carbon atom and the metal atom and fitted potential functions from the metal carbon cluster MC_n (M = Fe, Co, Ni; n = 1-4). In the case of metal-carbon bonding, D_e, R_e, β, b and δ are adjusted simultaneously for the error taking minima. The constructed parameters are listed in Table 1 (metal-metal) and Table 2 (metal-carbon).

3. Molecular dynamics simulation of the initial nucleation process of SWNTs

Clustering of carbon atoms with a transition metal cluster is modelled by the classical MD simulation using the above potential functions. The simulation technique is the same as in our previous report [10]. That is, it is assumed that a carbon source such as methane, ethanol or CO decomposes only at the catalytic surface and the decomposition and supply of a carbon atom take place immediately. This reaction process is expressed using a standard 6-12 Lennard-Jones potential, with the parameters ε = 2.5 meV and σ = 3.37 Å, between intermolecular carbon atoms, and using Brenner potential [17] for the covalent bonding between intramolecular carbon atoms in the catalyst.

In order to observe the growth process for a longer time scale within the computational limit,

the temperature and the density of carbon atoms in the system are much higher than in the experiment [6]. This is compensated for by a very rapid cooling technique [27] using the Berendsen thermostat [28]. Translational, rotational and vibrational temperatures of the cluster is independently controlled every 0.1 ps so that the difference between the control temperature and each individual temperature is reduced to 60%. The velocity Verlet method is employed to integrate the classical equation of motion with a time step of 0.5 fs. The actual simulation temperature does not correspond directly with that in the experimental study; however the relationship between these temperatures is examined in another paper [29].

We first prepare the initial transition metal clusters: Fe_{108}, Co_{108} and Ni_{108} by annealing face-centered cubic (FCC) crystal structures for 2 ns at 2000 K. The diameters of the obtained clusters are roughly 1.3 nm. As the initial condition, 500 carbon atoms and one of the obtained transition metal clusters are randomly allocated in a cubic periodic cell of $(20\ \mathrm{nm})^3$ (Fig. 3). The control temperature is set to 1500 K for subsequent simulations.

Figure 4 shows snapshots of calculations at 150 ns for Fe_{108}, Co_{108} and Ni_{108}, respectively. In the first stage, carbon atoms attach to the exposed surface and are absorbed into the cluster in every case. However, the Co cluster has partially a (111) crystal structure where metal atoms are regularly allocated and embedded in the hexagonal carbon networks after saturation at about 5 ns. Furthermore, the graphite structures gradually precipitate from the edge of the Co cluster. This implies a strong interaction between the graphite lattice and the metal atoms. The Ni cluster has a similar (111) structure. However, there is no allocated region in the Fe cluster, where carbon atoms cover the entire surface of the cluster. In the scale of this cluster, it is difficult to conclude the phase (solid or liquid) of the cluster because the effect of the surface is dominating.

Figure 5 shows a time series of the number of hexagonal and heptagonal rings in these clusters. The number of the hexagonal rings in the Co cluster increase about twice as fast as in the Fe cluster. This shows that the Co cluster has stronger graphitization action than the Fe cluster. This difference in graphitization action may reflect the ability to act as a catalyst in the formation process of SWNTs.

4. Potential energy fields made by FCC structure of transition metal atoms

As shown in Fig. 6(a), a hexagonal carbon network was formed after 150 ns as if the Co(111) surface were a template. It seems the potential energy surface made by Co(111) affects the formation of the hexagonal carbon network. When the bond length between metal atoms in an FCC crystal is 2.5 Å, the distance between centers of triangles made by the metal atoms in the FCC crystal is approximately 1.44 Å (Fig. 6(b)). This shows the FCC (111) structure can be a template from a geometrical standpoint. A recent TEM measurement [30] shows the {111} facet can be formed more easily on the Co particle in a SWNT nucleation point. That supports our simulation result, i.e. Co (111) surface works as a template for the hexagonal carbon network.

Here, the potential energy field felt by a carbon atom from a Co FCC structure is examined using above potential functions. 48 Co atoms are allocated in an x-y periodical cell as shown in Fig. 7. A bond length between Co atoms is set to 2.5 Å. The potential energy is calculated from Equations (1)-(3), and (5)-(9), using the above parameter sets in Table 1 and 2. The field is calculated to a distance of 3 Å from the (111) surface. Figure 7 shows the obtained potential energy field. The black lines in the boundary face show contour lines with an interval of 1 eV. The white surface shows a 3D contour surface around the minimum energy, -11.5 eV. The contour surface is distributed on the hexagonal network as in Fig. 6(b). Hence, a carbon atom prefers to stay the apex of hexagon.

Next, potential energy fields of three transition metals are compared using the above potential functions. Figure 8 shows potential fields made by FCC crystals of Fe, Co and Ni. As in Fig. 7, the black lines in the boundary face show contour lines with a 1eV interval. The white surface shows a 3D contour surface at -6.5 eV, which is the minimum energy for the Ni crystal case. Minimum energies for the Fe and the Co crystals are -10.0 eV and-11.5 eV, respectively. Therefore, the contour surfaces at -6.5 eV in the Fe and the Co system lie higher and wider than in the Ni system. This may result in the fact that Co has the strongest graphitization action among these three metals. In every case, the energy field exhibits local minima at the hexagon corners due to the geometry of the FCC structure. Therefore, carbon atoms tend to stay these regions. However, the stable structure of the small cluster is not straightforward.

5. Conclusion

The parameter set for transition metal carbide cluster is developed in the form of the bond-order type potential function. Using the potential function, clustering process of carbon atoms is studied by the MD simulation. The simulations show the Co cluster has a (111) surface that works as a template for making hexagonal carbon networks. In contrast, carbon atoms cover the entire surface in the case of the Fe cluster. This implies that the graphitic lattice interacts more strongly with Co atoms than with Fe atoms. The difference in the graphitization ability may reflect a metal's ability as a catalyst in the formation process of SWNTs.

Furthermore, potential energy fields are compared using potential functions based on constructed parameter sets. The minimum points of the potential energy fields are distributed on the hexagonal network. This ensures that FCC(111) works as a template in the formation process of hexagonal carbon networks. Comparison with PES made by DFT calculation may be important in the next stage.

Acknowledgements

Part of this work was financially supported by Grant-in-Aid for Research fellow of the JSPS (#15-11043). YS thanks Prof. T. Suzuki (Dept. of Materials Engineering, The University of Tokyo) for insightful discussions.

References

[1] S. Iijima, T. Ichihashi, Nature 363 (1993) 603.

[2] M.S. Dresselhaus, G. Dresselhaus, Ph. Avouris (Eds.), Carbon Nanotubes Synthesis, Structure, Properties, and Applications, Springer, Berlin, 2001.

[3] A. Thess, R. Lee, P. Nikolaev, H. Dai, P. Petit, J. Robert, C. Xu, Y.H. Lee, S.G. Kim, A. G. Rinzler, D. T. Colbert, G. E. Scuseria, D. Tománek, J. E. Fischer, R. E. Smalley, Science 273 (1996) 483.

[4] M. Yudasaka, R. Yamada, N. Sensui, T. Wilkins, T. Ichihashi, S. Iijima, J. Phys. Chem. B 103 (1999) 6224.

[5] Y. Zhang, Y. Li, W. Kim, D. Wang, H. Dai, Appl. Phys. A 74 (2002) 325.

[6] Y. Murakami, S. Chiashi, Y. Miyauchi, M. Hu, M. Ogura, T. Okubo, S. Maruyama, Chem. Phys. Lett. 385 (2004) 298.

[7] J. Gavillet, J. Thibault, O. Stéphan, H. Amara, A. Loiseau, Ch. Bichara, J.-P. Gaspard, F. Ducastelle, J. of Nanoscience and Nanotechnology 4 (2004) 346.

[8] J. Gavillet, A. Loiseau, C. Journet, F. Willaime, F. Ducastelle, J.-C. Charlier, Phys. Rev. Lett. 87 (2001) 275504.

[9] Y. Shibuta, S. Maruyama, Physica B 323 (2002) 187.

[10] Y. Shibuta, S. Maruyama, Chem. Phys. Lett. 382 (2003) 381.

[11] F. Ding, A. Rosén, K. Bolton, Chem. Phys. Lett. 393 (2004) 309.

[12] J.-Y. Raty, F. Gygi, F. Galli, Phys. Rev. Lett. 95 (2005) 096103.

[13] R.S. Wagner, W.C. Ellis, Appl. Phys. Lett. 4 (1964) 89.

[14] C.J. Smithells, E.A. Brandes, G.B. Brook, Smithells Metal Reference Book 7th edition, Butterworth-Heinimann, London, 1992.

[15] P.M. Morse, Phys. Rev. 34 (1929) 57.

[16] L.A. Girifalco, V.G. Weizer, Phys. Rev. 114 (1959) 687.

[17] R. A. Johnson, J. Phys. F: 3 (1973) 295.

[18] M.W. Finnis, J.E. Sinclair, Philosophical Magazine A, 50 (1984) 45.

[19] M.S. Daw, M.I Baskes, Phys. Rev. B 29 (1984) 6443.

[20] Y. Yamaguchi, S. Maruyama, Euro. Phys. J. D 9 (1999) 385.

[21] D.W. Brenner, Phys. Rev. B 42 (1990) 9458.

[22] M. J. Frisch, G. W. Trucks, H. B. Schlegel, G. E. Scuseria, M. A. Robb, J. R. Cheeseman, V. G. Zakrzewski, J. A. Montgomery, Jr., R. E. Stratmann, J. C. Burant, S. Dapprich, J. M. Millam, A. D. Daniels, K. N. Kudin, M. C. Strain, O. Farkas, J. Tomasi, V. Barone, M. Cossi, R. Cammi, B. Mennucci, C. Pomelli, C. Adamo, S. Clifford, J. Ochterski, G. A. Petersson, P. Y. Ayala, Q. Cui, K. Morokuma, D. K. Malick, A. D. Rabuck, K. Raghavachari, J. B. Foresman, J. Cioslowski, J. V. Ortiz, A. G. Baboul, B. B. Stefanov, G. Liu, A. Liashenko, P. Piskorz, I. Komaromi, R. Gomperts, R. L. Martin, D. J. Fox, T. Keith, M. A. Al-Laham, C. Y. Peng, A. Nanayakkara, M. Challacombe, P. M. W. Gill, B. Johnson, W. Chen, M. W. Wong, J. L. Andres, C. Gonzalez, M. Head-Gordon, E. S. Replogle, and J. A. Pople, Gaussian 98, Revision A.9, Gaussian, Inc., Pittsburgh PA, 1998.

[23] A.D. Beche, J. Chem. Phys. 98 (1993) 5648.

[24] C. Lee, W. Yang, R.G. Parr. Phys. Rev. B 37 (1988) 785.

[25] P.J. Hay, W.R. Wadt, J. Chem. Phys. 82 (1985) 270.

[26] M .Castro, C. Jamorski, D.R. Salahub, Chem. Phys. Lett., 271 (1997) 133.

[27] Y. Yamaguchi, S. Maruyama, Chem. Phys. Lett. 286 (1998) 336.

[28] H.J.C. Berendsen, J.P.M. Postma, W. F. van Gunsteren, A. DiNola, J. R. Haak, J. Chem, Phys. 81 (1984) 3684.

[29] S. Maruyama, Y. Yamaguchi, Chem. Phys. Lett., 286 (1998) 343.

[30] H. Zhu, K. Suenaga, A. Hashimoto, K. Urita, K. Hata, S. Iijima, Small 12 (2005) 1180.

Figure Captions

Fig. 1 Geometrical Structure of M_n and MC_n clusters.

Fig. 2 Fitted potential functions from the lowest ground state by B3LYP/LANL2DZ. Dots represent the binding energies from DFT calculations. Fitted line is determined from the steepest descent method.

(a) Fitted potential functions for metal-metal bonds

(b) Fitted potential functions for metal-carbon bonds

Fig. 3 An initial condition for modelling of the CCVD process. Large spheres represent metal atoms and small ones represent carbon atoms. 500 carbon atoms and a metal cluster are allocated randomly in the 20 nm periodic cubic cell.

Fig. 4 Snapshots of the Fe_{108}, Co_{108} and Ni_{108} clusters in the 150 ns calculation of the clustering process of carbon atoms. For clarity, carbon atoms are not shown.

Fig. 5 Time series of the number of hexagonal and pentagonal rings in Fe_{108}, Co_{108} and Ni_{108} clusters in the 150 ns calculation of the clustering process. The number of the hexagonal rings in the Co cluster increase about twice as fast as in the Fe cluster.

Fig. 6 Co_{108} cluster obtained after 150 ns calculation. Co atoms are regularly allocated and embedded in the hexagonal carbon network.

(a) The graphitic structure in the Co cluster after 150 ns calculation.

(b) Depiction of the hexagonal rings.

Fig. 7 3D contour mapping of the potential energy field of an FCC crystal of Co atoms as felt by a carbon atom. Black lines on the boundary face represent contour lines with an interval of 1 eV. The white surface represents the contour surface at -11.5 eV.

Fig. 8 Comparison of the 3D contour maps of the potential energy fields felt by a carbon atom from FCC crystals of Fe, Co and Ni atoms. Black lines on the boundary face represent contour lines with a 1 eV interval. The white surface represents the contour surface at -6.5 eV.

Table 1. Potential parameters for metal-metal interactions.

	S	β(1/Å)	D_{e1}(eV)	D_{e2}(eV)	C_D	R_{e1}(Å)	R_{e2}(Å)	C_R	R_1(Å)	R_2(Å)
Fe-Fe	1.3	1.2173	0.4155	0.8392	0.8730	2.627	0	-	2.7	3.2
Co-Co	1.3	1.5552	0.4311	1.0230	0.6413	2.5087	0.1660	0.3770	2.7	3.2
Ni-Ni	1.3	1.5700	0.4217	1.0144	0.8268	2.4934	0.1096	0.3734	2.7	3.2

Table 2. Potential parameters for metal-carbon interactions.

	D_e(eV)	S	β(1/Å)	R_e(Å)	R_1(Å)	R_2(Å)	b	δ
Fe-C	3.3249	1.3	1.5284	1.7304	2.7	3.0	0.0656	-0.4279
Co-C	3.7507	1.3	1.3513	1.6978	2.7	3.0	0.0889	-0.6256
Ni-C	2.4673	1.3	1.8706	1.7628	2.7	3.0	0.0688	-0.5351

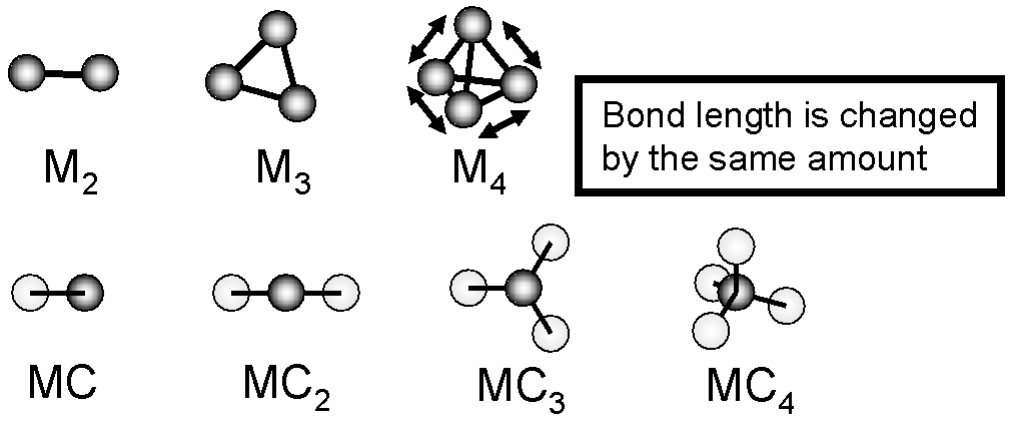

Y. Shibuta, S. Maruyama, Fig. 1

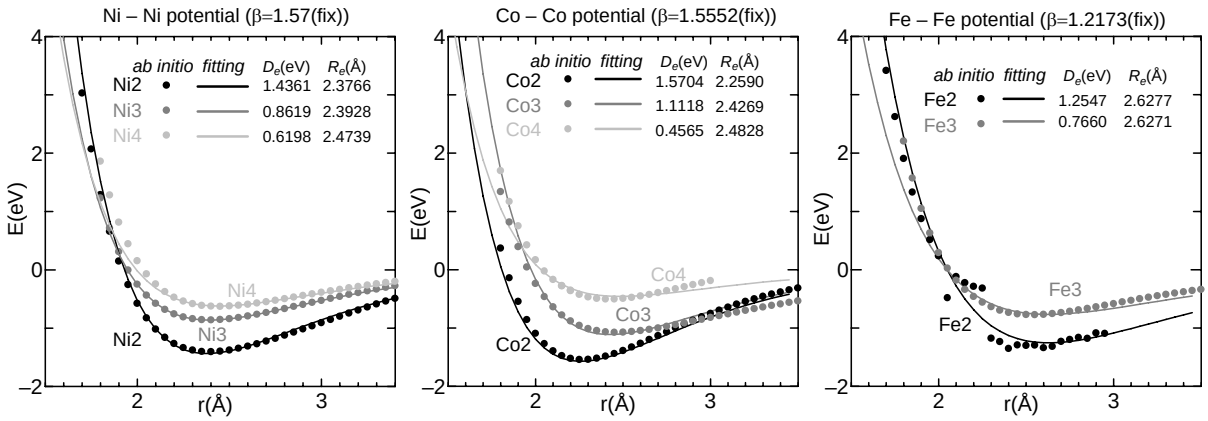

(a) Fitted potential functions for metal-metal bonds

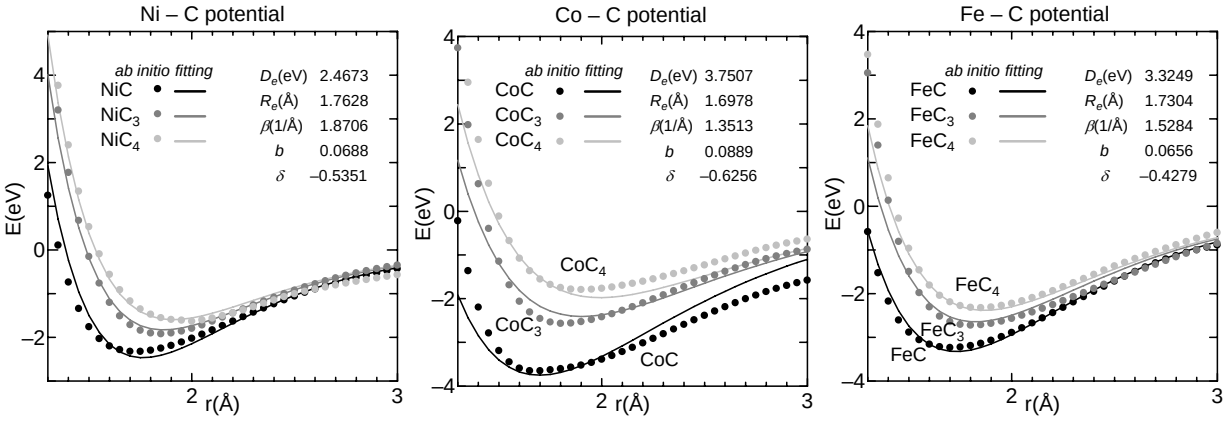

(b) Fitted potential functions for metal-carbon bonds

Y. Shibuta, S. Maruyama, Fig. 2

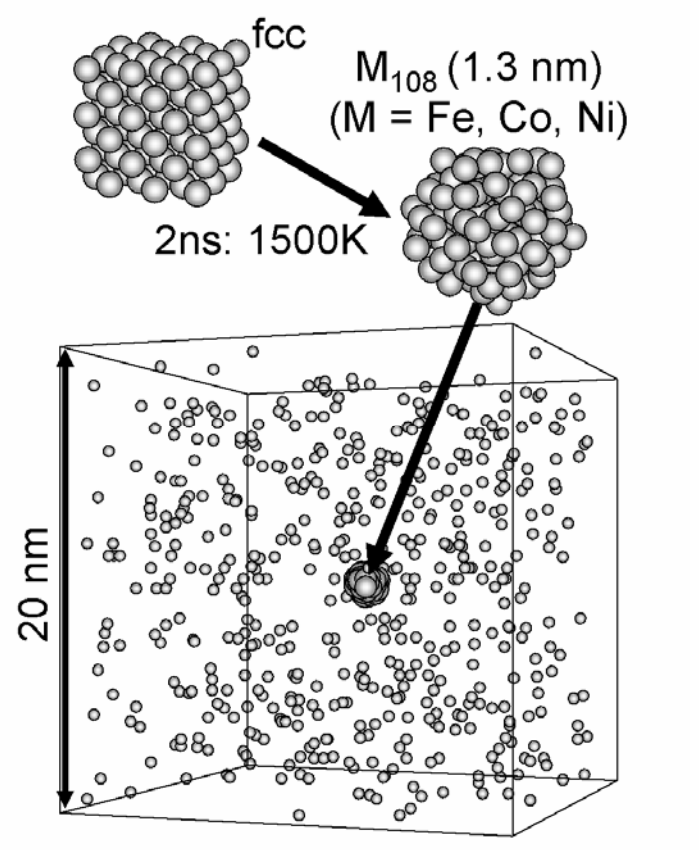

Y. Shibuta, S. Maruyama, Fig. 3

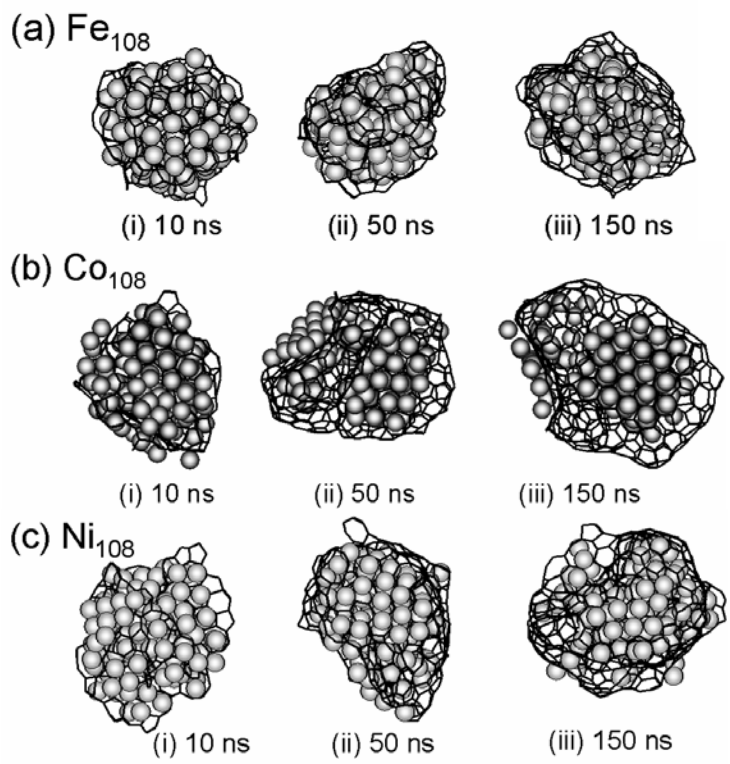

Y. Shibuta, S. Maruyama, Fig. 4

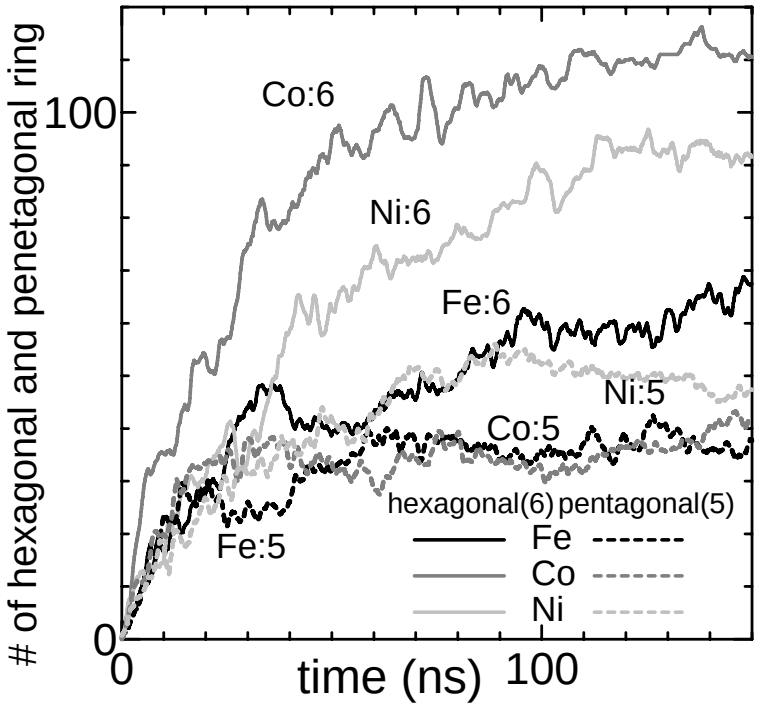

Y. Shibuta, S. Maruyama, Fig. 5

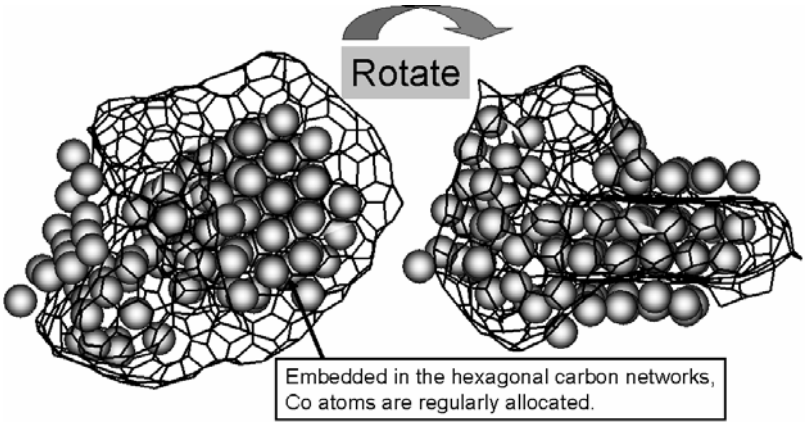

(a) A graphitic structure in the Co cluster after 150 ns calculation

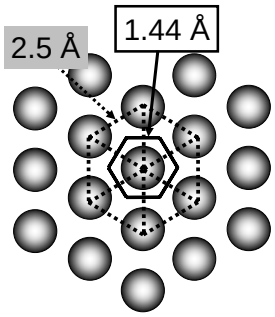

(b) Depiction of the hexagonal rings

Y. Shibuta, S. Maruyama, Fig. 6

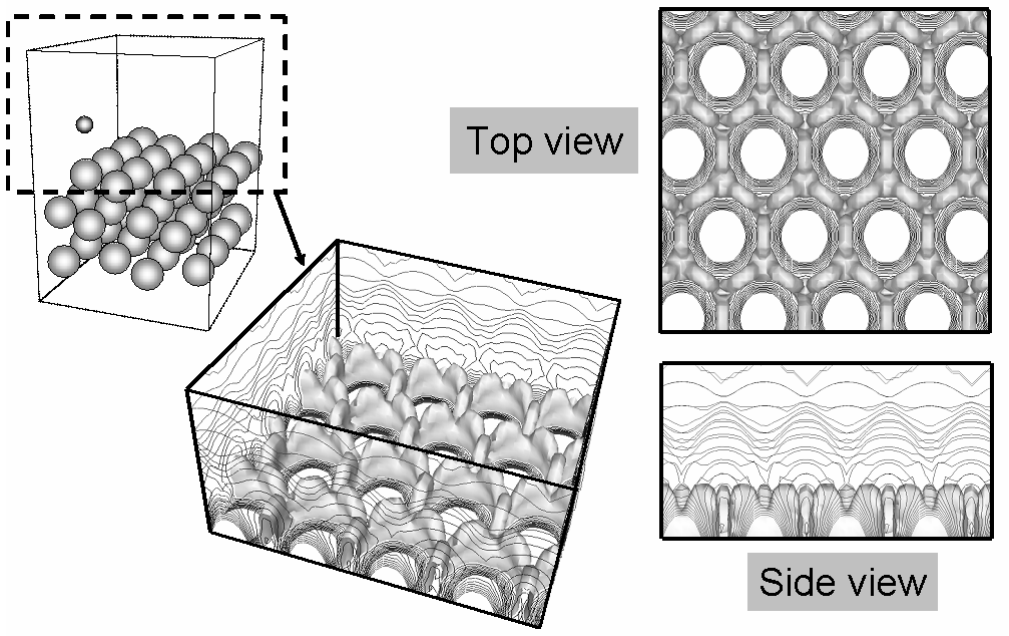

Y. Shibuta, S. Maruyama, Fig. 7

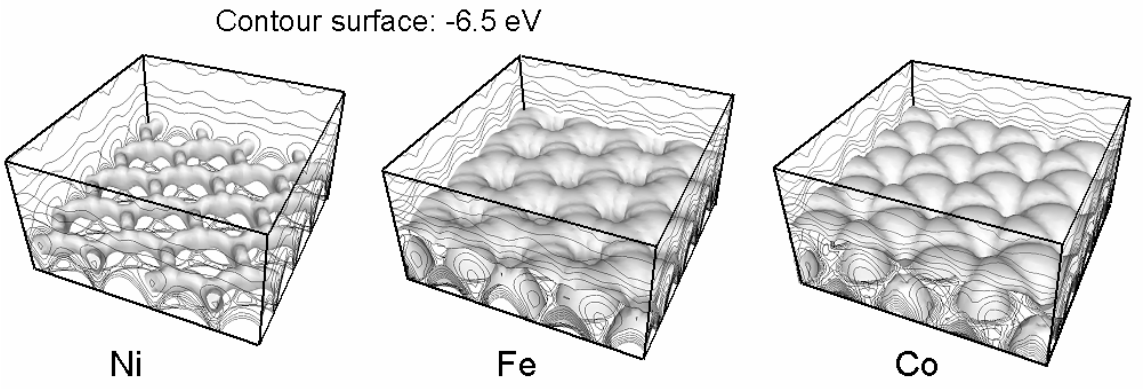

Y. Shibuta, S. Maruyama, Fig. 8